Wave Motion 122 (2023) 103190

Contents lists available at ScienceDirect

Wave Motion

journal homepage: www.elsevier.com/locate/wamot

Steady-state hydroelastic waves generated by a moving load in a uniform current

P. Wang [a], D.Q. Lu [b,c,d,*], L.D. Fu [a]

[a] School of Mathematics and Physics, Qingdao University of Science and Technology, Songling Road, Qingdao 266061, China
[b] Shanghai Institute of Applied Mathematics and Mechanics, School of Mechanics and Engineering Science, Shanghai University, Yanchang Road, Shanghai 200072, China
[c] Shanghai Key Laboratory of Mechanics in Energy Engineering, Yanchang Road, Shanghai 200072, China
[d] Shanghai Institute of Aircraft Mechanics and Control, Zhangwu Road, Shanghai 200092, China

ARTICLE INFO

Article history:
Received 3 March 2023
Received in revised form 1 July 2023
Accepted 7 July 2023
Available online 20 July 2023

Keywords:
Steady-state hydroelastic waves
Moving load
Uniform current
Homotopy analysis method (HAM)

ABSTRACT

Steady-state hydroelastic waves generated by a moving load with a uniform current are investigated analytically in the framework of nonlinear potential theory. Considering the load with an exponential distribution in horizontal direction, we focus on the wave dynamics characteristics when the relative current speed or the nonlinearity increases. With the aid of the homotopy analysis method (HAM), appropriate solution expressions for the unknown variables are established by comparing the relative current speed U and the minimal phase speed $c_{\min}$ of the hydroelastic waves. Our results demonstrate that, the wave deflection is symmetric about the load if U is much smaller than $c_{\min}$. The wave deflection becomes more oscillatory and its amplitudes increase in the vicinity of the load when U increasingly approaches $c_{\min}$. If U is greater than $c_{\min}$, the hydroelastic waves will be generated far away from the load, and the period of the gravity waves in the downstream region are relatively larger than those of the hydroelastic waves in the upstream region. As U increases continuously, the amplitudes of gravity and hydroelastic waves all first increase and then decrease. It should be noted that there is a larger $c_{\min}$ of the approximate nonlinear dispersion relation than that of the linear one, and the variation of the nonlinear wave deflection would be underestimated if the linear dispersion relation is used. Finally, the graphical representations show the effects of several important physical parameters including the uniform current speed, the amplitude of incident wave, and the plate thickness on the hydroelastic waves.

1. Introduction

Hydroelastic waves (namely flexural–gravity waves), which are generated due to the elastic deformation of a very large floating structure (VLFS) or an floating ice sheet in the ocean, have been an important topic in water wave field for many decades. One fundamental interest for operational safety is the dynamic characteristics of the waves due to an external load, which may describe the impact of vehicles or aircrafts on the VLFS or the ice sheet.

The generation of linear hydroelastic waves due to an external load has been well studied in recent decades. Wilson [1] firstly developed a simple theory for the coupling between a moving load and the flexural waves traveling in a floating

* Corresponding author at: Shanghai Institute of Applied Mathematics and Mechanics, School of Mechanics and Engineering Science, Shanghai University, Yanchang Road, Shanghai 200072, China.
E-mail addresses: dqlu@shu.edu.cn, dqlu@graduate.hku.hk (D.Q. Lu).

https://doi.org/10.1016/j.wavemoti.2023.103190
0165-2125/

ice sheet. He found the minimum wave velocity is a critical one which is a threshold for the existence of flexural waves. Steady wave patterns due to a uniform moving source was considered by Davys et al. [2] with the help of asymptotic Fourier analysis to find that the short elastic waves propagate upstream while the long gravity waves appear downstream. Schulkes and Sneyd [3] derived an exact expression for the ice deflection due to an impulsively concentrated line load to investigate time-dependent effects. Milinazzo et al. [4] considered a uniform rectangular load distribution, and showed the amplitude of the ice displacement depends on the aspect ratio of the load, which is in good agreement with the experimental results. A comprehensive summary on hydroelastic deflection of an ice sheet due to the moving loads has been systematically described in Squire's monograph [5].

The flexural–gravity wave resistances due to a surface-moving line source was considered by Lu and Zhang [6] who found that, when the moving speed of the source is greater than the minimum phase speed, the wave resistances firstly increase to their peak values and then decrease. A further study on the transient flexural–gravity waves due to an impulsive source was conducted by Lu and Sun [7] for a two-layer density-stratified fluid. They found that the profiles of both surface and interfacial waves depend on the moving speed of the observer in the relation to the maximal and minimal group velocities. Li and Lu [8] modeled the VLFS as a thin viscoelastic plate to study the response of the flexural–gravity wave due to a load steadily moving or suddenly accelerated along a rectilinear orbit. Meylan [9] studied the time-dependent deflection of a floating elastic plate subject to a transient force by the eigenfunction matching method, and showed detailedly how the solution in two dimensions can be extended to three dimensions with little modification of the underlying numerical method. Latterly, the hydroelastic symmetric response of an ice sheet caused by a pressure moving either in the ice lead or on the infinite ice sheet with a crack was investigated by Xue et al. [10]. It is found that the load speeds determine the maximum deflection of an ice cover, the maximum stress in the ice, and the maximum wave-making resistance.

These aforementioned works are in the scope of linear wave theory under the assumption that the wave amplitude is very small in comparison with the wavelength. So these linear models are not suitable to describe large-amplitude hydroelastic wave deflections. Părău and Dias [11] preliminary studied the nonlinear and steady response of an ice sheet to a concentrated line load, and analyzed the deflection of solitary waves when the load speed is close to the minimal phase speed $c_{\min}$. Bonnefoy et al. [12] calculated the nonlinear response of an infinite ice sheet to a moving load by using a higher-order spectral method, and compared their nonlinear solution with the linear one. It is found that there is a good agreement with both solutions in the appropriate regimes. Părău and Vanden–Broeck [13] considered three-dimensional nonlinear waves beneath an ice sheet due to a steadily moving pressure by using a boundary integral equation method, and discussed different types of responses of the floating ice sheet with the variation of the moving pressure speed. Guyenne and Părău [14] considered forced flexural–gravity solitary waves generated by a moving load for the nonlinear problem as proposed by Plotnikov and Toland [15]. They obtained the Hamiltonian formulation for three-dimensional fully nonlinear flexural–gravity waves.

All the investigations mentioned above were under the hypothesis that there is no current in the ocean. As we know, there are various reasons such the changes in the wind direction and force, the tidal forces of the sun or moon, the earth's gravity which can generate the ocean current. Thus, it is important to study the effect of the underlying current on the hydroelastic wave. However, due to the complexity of wave–current–structure interaction, the current is usually neglected which may lead to erroneous results. The hydroelastic waves in the presence of both an external load and an underlying current have been studied by few researchers. Mohanty et al. [16] studied a combined effect of current and compressive force on time-dependent flexural–gravity wave motion in both the cases of single- and two-layer fluids by analyzing the dispersion relation, phase and group velocities. Lu and Yeung [17] considered unsteady flexural gravity waves on a thin elastic plate caused by the interaction of fixed concentrated line loads and the underlying current. For the steady response, an explicit expression was derived by the residue theorem. It is found that the flexural–gravity wave motion depends on the ratio of current speed to phase or group speeds.

In the present paper, our objective is to investigate analytically the nonlinear and steady hydroelastic waves generated by a moving load in a uniform current with the aid of the homotopy analysis method (HAM) developed by Liao [18–20]. It mainly extends the work of Lu and Yeung [17] from the small-amplitude hydroelastic wave to the nonlinear large-amplitude one. Detailed research is organized as follows. The mathematical model is formulated in Section 2. In Section 3.1, in the frame of HAM, deformation equations including the zero-order deformation equations and the high-order deformation equations are deduced. In Section 3.2, the approximate nonlinear dispersion relation is derived and then solution expressions and initial guesses are constructed accordingly by comparing the relative current speed and the minimal phase speed. In Section 3.3, we present explicitly the first-order HAM-based analytical solutions for the hydroelastic wave elevation and the velocity potential. The variation of the wave deflections with the increased nonlinearity and two important physical parameters are discussed in Section 4. Concluding remarks follow in Section 5.

2. Mathematical formulation

A train of steady-state hydroelastic waves generated by a moving load with a constant speed V_0 in a uniform current U_0 is considered for the two-dimensional case in the earth-fixed coordinate system. We choose a Coordinate System oxz fixed on the moving load. As illustrated in Fig. 1, Cartesian Coordinate are defined with the z-axis pointing upwards and $z = 0$ at the undisturbed plate–water interface. The floating elastic plate extends to the infinity along the x-axis, and an underlying current is assumed to be moving toward the positive x-axis.

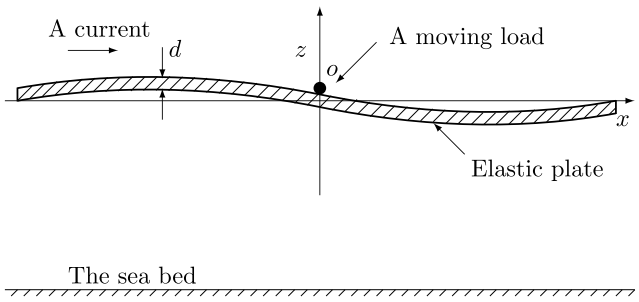

Fig. 1. Coordinates.

Let $\phi(x, z)$ denote the potential for the disturbed velocity, and $\zeta(x)$ the hydroelastic wave elevation at the fluid–plate interface. Assuming that the fluid is inviscid and incompressible and the flow is irrotational, we have Laplace's equation

$$\nabla^2\phi = 0, \qquad (z \le \zeta(x)), \tag{1}$$

subject to the bottom condition at deep water

$$\frac{\partial\phi}{\partial z} = 0, \qquad (z = -\infty), \tag{2}$$

Let ρ be the uniform densities of the fluid, g the gravitational acceleration, and $U = U_0 - V_0$ the relative uniform current speed. The surface tension is neglected. Then the two nonlinear boundary conditions on the unknown plate–water interface ($z = \zeta(x)$) read

$$\mathcal{N}_1[\phi, \zeta] = U^2\frac{\partial^2\phi}{\partial x^2} + g\frac{\partial\phi}{\partial z} + U\frac{\partial f}{\partial x} - g\frac{\partial\phi}{\partial x}\frac{\mathrm{d}\zeta}{\mathrm{d}x} + \frac{U}{\rho}\left(D\frac{\mathrm{d}^5\zeta}{\mathrm{d}x^5} + \frac{\mathrm{d}P_{\text{ext}}}{\mathrm{d}x}\right) = 0, \tag{3}$$

$$\mathcal{N}_2[\phi, \zeta] = f + U\frac{\partial\phi}{\partial x} + g\zeta + \frac{1}{\rho}\left(D\frac{\mathrm{d}^4\zeta}{\mathrm{d}x^4} + P_{\text{ext}}\right) = 0, \tag{4}$$

with $f = |\nabla\phi|^2/2$. $\mathcal{N}_1[\cdot,\cdot]$ and $\mathcal{N}_2[\cdot,\cdot]$ are the nonlinear differential operators in the frame of HAM. The elaborated derivation for the conditions (3) and (4) are given in Appendix A. In Eqs. (3) and (4), $D = Ed^3/[12(1-\nu^2)]$ is the flexural rigidity of the plate in which E, d and ν are Young's modulus, the constant thickness, and Poisson's ratio of the plate, respectively. P_{ext} the external pressure distribution of a localized load at the coordinate origin.

Following Părău and Vanden-Broeck [13], we describe the pressure distribution which decays exponentially with horizontal distance from the load as

$$P_{\text{ext}}(x) = \begin{cases} P_0 \mathrm{e}^{L^2/(x^2-L^2)}, & |x| < L, \\ 0, & \text{otherwise}, \end{cases} \tag{5}$$

where P_0 is a constant magnitude of the pressure, L is the size of the support of the pressure.

The unknown velocity potential $\phi(x, z)$ and hydroelastic waves $\zeta(x)$ are obtained from Eqs. (1)–(5) by using the HAM in the subsequent sections.

3. Approximate analytical solution approach

3.1. Deformation equations

The HAM is a semi-analytic approximation method which has successfully been applied to solve some highly nonlinear hydrodynamic problems [21–24]. On basis of the HAM, we first construct two homotopies $\Phi(x, z; q)$ and $\eta(x; q)$ which are governed by a new family of nonlinear partial differential equations (PDEs) corresponding to the Eqs. (1)–(4) as

$$\nabla^2\Phi = 0, \qquad (z \le \eta), \tag{6}$$

$$\frac{\partial\Phi}{\partial z} = 0, \qquad (z = -\infty), \tag{7}$$

$$(1-q)\mathcal{L}_1[\Phi - \phi_0] = qC_0\mathcal{N}_1[\Phi, \eta], \qquad (z = \eta), \tag{8}$$

$$(1-q)\mathcal{L}_2[\eta - \zeta_0] = qC_0\mathcal{N}_2[\Phi, \eta], \qquad (z = \eta), \tag{9}$$

where C_0 is a nonzero convergence-control parameter and $q \in [0, 1]$ the embedding parameter. $\phi_0(x, z)$ and $\zeta_0(x)$ are the initial guesses of the velocity potential $\phi(x, z)$ and the hydroelastic wave deflection $\zeta(x)$, respectively. As the parameter

q increases from 0 to 1, the homotopy $\Phi(x,z;q)$ deforms continuously from its initial estimation $\phi_0(x,z)$ to the exact solution $\phi(x,z)$, and the homotopy $\eta(x;q)$ varies continuously from $\zeta_0(x)$ to $\zeta(x)$. Eqs. (8) and (9) are called the zero-order deformation equations in the HAM.

We choose the linear terms in $\mathcal{N}_1[\cdot,\cdot]$ as an auxiliary linear operator for $\Phi(x,z;q)$

$$\mathcal{L}_1[\Phi(x,z;q)] = U^2\frac{\partial^2\Phi}{\partial x^2} + g\frac{\partial\Phi}{\partial z} = g\left(L_0\frac{\partial^2\Phi}{\partial x^2} + \frac{\partial\Phi}{\partial z}\right), \tag{10}$$

and the linear terms in $\mathcal{N}_2[\cdot,\cdot]$ as another linear operator for $\eta(x;q)$

$$\mathcal{L}_2[\eta(x;q)] = \frac{D}{\rho}\frac{\mathrm{d}^4\eta}{\mathrm{d}x^4} + g\eta = g\left(\gamma\frac{\mathrm{d}^4\eta}{\mathrm{d}x^4} + \eta\right), \tag{11}$$

where $\mathcal{L}_n[0]=0$, $(n=1,2)$, $L_0 = U^2/g$ and $\gamma = D/\rho g$.

We expand the two unknown variables $\Phi(x,z;q)$ and $\eta(x;q)$ into the Maclaurin series with respect to q

$$\Phi(x,z;q) = \sum_{m=0}^{+\infty}\phi_m(x,z)q^m, \tag{12}$$

$$\eta(x;q) = \sum_{m=0}^{+\infty}\zeta_m(x)q^m, \tag{13}$$

where

$$\{\phi_m(x,z),\zeta_m(x)\} = \frac{1}{m!}\frac{\partial^m}{\partial q^m}\{\Phi(x,z;q),\eta(x;q)\}\Big|_{q=0}. \tag{14}$$

The unknown $\phi_m(x,z)$ and $\zeta_m(x)$ are governed by the following high-order deformation equations

$$\mathcal{L}_1[\phi_m]|_{z=0} = C_0\Delta^{\phi}_{m-1} - \bar{S}_m + H_m S_{m-1}, \tag{15}$$

$$\mathcal{L}_2[\zeta_m] = C_0\Delta^{\zeta}_{m-1} + H_m g\left(\gamma\frac{\mathrm{d}^4\zeta_{m-1}}{\mathrm{d}x^4} + \zeta_{m-1}\right), \tag{16}$$

where $H_m = \mathrm{H}(m-2)$, and $\mathrm{H}(\cdot)$ is the Heaviside step function. The elaborated expressions for Δ^{ϕ}_{m-1}, $\bar{S}_m$, S_{m-1}, and Δ^{ζ}_{m-1} are given in Appendix B.

It is noted that the nonlinear zeroth-order deformation Eqs. (8) and (9) are defined on the unknown boundary $z=\eta(x;q)$ while the linear high-order deformation Eqs. (15) and (16) are defined on the fixed boundary $z=0$. Thus, these linear and decoupled high-order deformation equations can easily be adapted for symbolic computation.

3.2. Solution expressions and initial guesses

The linear dispersion relation is derived from the linearized approximation [6,13,25]

$$\omega^2 = gk\left(\frac{\gamma k^4+1}{\sigma k+1}\right), \tag{17}$$

where $\sigma = M_{\mathrm{e}}/\rho_{\mathrm{e}}$. k and ω are the wave number and the angular frequency of the linear hydroelastic waves, respectively. M_{e} is the mass per unit area of the elastic plate and ρ_{e} is the plate density.

The aforementioned researches on the nonlinear hydroelastic waves due to a concentrated load [11–14] were usually based on the assumption that the dispersion relation is linear in order to simplify calculation. However, the actual wave frequency Ω of the nonlinear hydroelastic waves is different from the linear frequency ω and the linear dispersion relation (17) is not valid for large-amplitude waves [22,24]. So we introduce

$$\Omega/\omega = \varepsilon, \tag{18}$$

the dimensionless parameter ε is a constant larger than 1. The nonlinearity of the dispersion relation strengthens as ε increases.

We restrict our attention to the steady hydroelastic waves and then the term σk in Eq. (17) is neglected. So the phase speed for nonlinear hydroelastic waves is represented as follows

$$c = \frac{\Omega}{k} = \varepsilon\sqrt{\frac{g}{k}\left(\gamma k^4+1\right)}, \tag{19}$$

and it always has a minimum $c_{\min} = 2\varepsilon\left(Dg^3/27\rho\right)^{1/8}$.

We adopt physical parameters given by Squire et al. [5]: $E = 5\times10^9$ N m^{-2}, $\rho_{\mathrm{e}} = 917$ kg m^{-3}, $\nu = 1/3$, $\rho = 1024$ kg m^{-3}, and take these data hereinafter for computation unless otherwise stated. Fig. 2 shows the hydroelastic

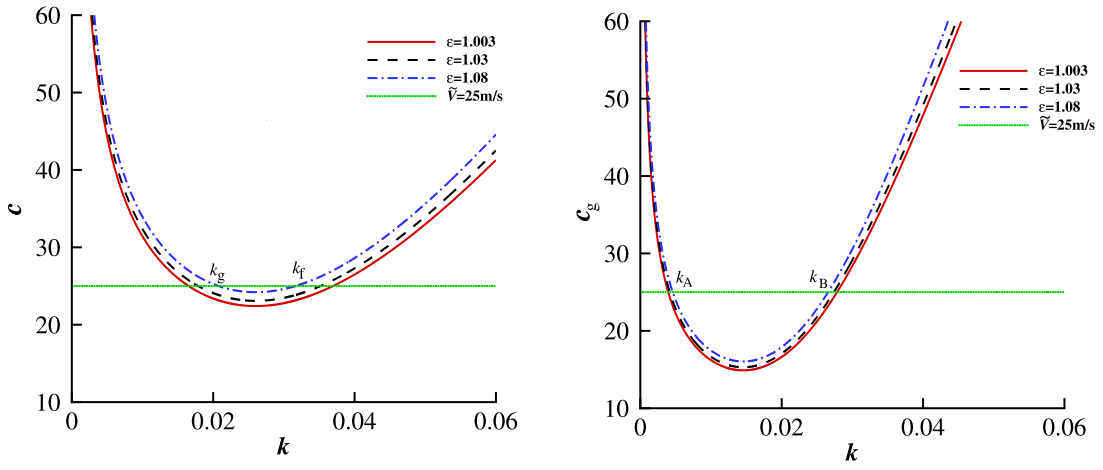

(a) Phase speed c (b) Group velocity c_g

Fig. 2. The phase speed and group velocity in deep water versus the wave number k for different dimensionless frequency ε.

wave speed $c(k)$ and group speed $c_g(k)$ versus the wave number k for different dimensionless frequency ε. It is found that there are a minimal phase speed and a minimal group speed. For example, as $\varepsilon = 1.003$, $c_{\min} = 22.48$ m s^{-1} and $c_{g\min} = 14.91$ m s^{-1}.

Considering the linear hydroelastic wave is mainly determined by the relationship between U and $c(k)$ or $c_g(k)$ [6,7,17], we construct the solution expressions of every order hydroelastic wave elevation and every order velocity potential as the superposition of linear corresponding solutions

$$\phi_m(x,z) = \sum_{n=1}^{N_1}\sum_{i=1}^{2} \gamma_i \alpha_{i,m,n} \exp(nk_i z)\sin(nk_i x), \tag{20}$$

$$\zeta_m(x) = \sum_{n=0}^{N_2}\sum_{i=1}^{2} \gamma_i \beta_{i,m,n} \cos(nk_i x), \tag{21}$$

respectively, where γ_1 and γ_2 are given parameters which satisfy $\gamma_1 + \gamma_2 = 1$ $(0 \le \gamma_1, \gamma_2 \le 1)$; $\alpha_{i,m,n}$ and $\beta_{i,m,n}$ are coefficients to be determined; N_1 and N_2 are positive integers. As $U > c_{\min}$, $\gamma_1 = 1$, $\gamma_2 = 0$ and $k_1 = k_g$ for $x < 0$ while $\gamma_1 = 0$, $\gamma_2 = 1$ and $k_2 = k_f$ for $x > 0$, in which k_g and k_f are the small and large real roots of $c - U = 0$, respectively, as shown in Fig. 2(a). As $U < c_{\min}$, $0 < \gamma_1, \gamma_2 < 1$, $k_1 = k_A$ and $k_2 = k_B$ in which k_A and k_B are the small and large real roots of $c_g - U = 0$, respectively, and c_g is the group velocity, as shown in Fig. 2(b). In the linear wave system, k_1 and k_2 represent the gravity-dominated and elasticity-dominated wave, respectively [6,7,17].

According to the solution expression expressions (20) and (21), to simplify the subsequent solution procedure, we construct the initial approximations for the unknown variables as

$$\phi_0(x,z) = \sum_{i=1}^{2} \gamma_i \alpha_{i,0,1} \exp(k_i z)\sin(k_i x), \tag{22}$$

$$\zeta_0(x) = 0, \tag{23}$$

where $\alpha_{i,0,1}$ is a coefficient to be determined.

3.3. Iteration of approximated solutions

We expand approximately the pressure function (5) into cosine series with the periodic extension

$$P_{\text{ext}}(x) = \begin{cases} \dfrac{P_0}{\mathrm{e}}\left[\dfrac{2}{3} + \dfrac{4}{\pi^2}\displaystyle\sum_{n=1}^{+\infty}\dfrac{(-1)^{n-1}}{n^2}\cos\left(\dfrac{n\pi x}{L}\right)\right], & |x| < L, \\ 0, & \text{otherwise.} \end{cases} \tag{24}$$

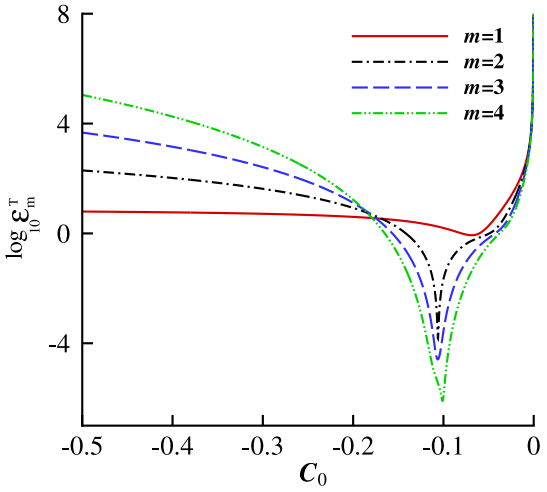

Fig. 3. Logarithm of the squared residual $\log_{10}\varepsilon_m^{\mathrm{T}}$ of the mth order homotopy approximation versus C_0 in the trailing regions of the point load when $U = 10$ m s^{-1}.

We choose $n = 5$ in the following calculations. It is noted that, following Liao [18–20], we add a relation equation as follows to make our model closed

$$\max \zeta_1(x) - \min \zeta_1(x) = 2H, \tag{25}$$

where H is the amplitude of the first-order incident wave.

Substituting the solution expression expressions (20) and (21), the two guesses (22) and (23), the series (24) and the relation Eq. (25) into the high-order deformation equations, we can obtain these coefficients of the solution expressions, and the one-order functions $\phi_1(x, z)$ and $\zeta_1(x)$ with analytical expressions for $\alpha_{i,1,0}$, $\alpha_{i,1,n}$, $\beta_{i,1,0}$ and $\beta_{i,1,n}$ $(n = 1, 2, \ldots, 5)$ given in Appendix C.

To obtain the convergent HAM-based series solutions by choosing the optimal C_0, we construct the total residual square error

$$\varepsilon_m^{\mathrm{T}} = \frac{1}{1+M}\sum_{i=0}^{M}\left[\left(\mathcal{N}_1[\Phi,\eta]\big|_{x=i\triangle x,q=1}\right)^2 + \left(\mathcal{N}_2[\Phi,\eta]\big|_{x=i\triangle x,q=1}\right)^2\right], \tag{26}$$

which is the sum of the residual square error of the zeroth-order deformation Eqs. (8) and (9) at $q = 1$, (i.e., the boundary conditions (3) and (4)). $\triangle x = x^*/M$ where x^* is the value range of x and M is an integer. We choose $x^* = 800$ m and $M = 10$ hereinafter, and obtain the optimal convergence control parameter C_0 by the minimal $\varepsilon_m^{\mathrm{T}}$ in residual plot, as shown in Fig. 3.

4. Results and analysis

To show the validity and convergence of our HAM-based series solutions, we illustrate, in the trailing region of the localized load, the total squared residuals $\varepsilon_m^{\mathrm{T}}$ at several different orders versus C_0 with the case of $d = 2.5$ m, $H = 0.2$ m, $U = 10$ m s^{-1}, $kL = \pi$, $\varepsilon = 1.003$, $P_0 = 3000$ Pa and other physical parameters given by Squire et al. [5]. As shown in Fig. 3, it is found that $\log_{10}\varepsilon_m^{\mathrm{T}}$ at every order has the smallest value, and $\log_{10}\varepsilon_m^{\mathrm{T}}$ decreases quickly when the order m increases in the interval $-0.2 < C_0 < 0$. So, we choose the optimal convergence-control parameter $C_0 = -0.1$. For example, as $m = 6$, the smallest value of $\varepsilon_6^{\mathrm{T}}$ is 3.216×10^{-8} in Table 1. It is demonstrated that our HAM-based solutions are highly convergent and accurate.

Fig. 4 illustrates the variations of the phase speed c and the group velocity c_{g} versus the wave number k for several different Young's moduli E and different plate thicknesses d. It can been seen that, as E or d increases, both the linear $(\varepsilon = 1)$ and nonlinear $(\varepsilon > 1)$ phase speed c rise. Moreover, for every same E or d, the nonlinear phase speed c or the group velocity c_{g} is always greater than that for the linear one. So the variations of the nonlinear wave deflection would be underestimated if the linear dispersion relation is used.

The effects of several important physical parameters on the waves are considered. We firstly consider, at the same ε, the impact of the current speed U by increasing U from 0 m s^{-1} to 35 m s^{-1}. Fig. 5 shows that the variation of the plate deflection depends on U.

As the current speed U is much smaller than the minimal phase speed $c_{\min}$, the plate deflection occurs near the localized load with $x = 0$ and is symmetric about the load. This is because there is a static deflection of a very large floating structure

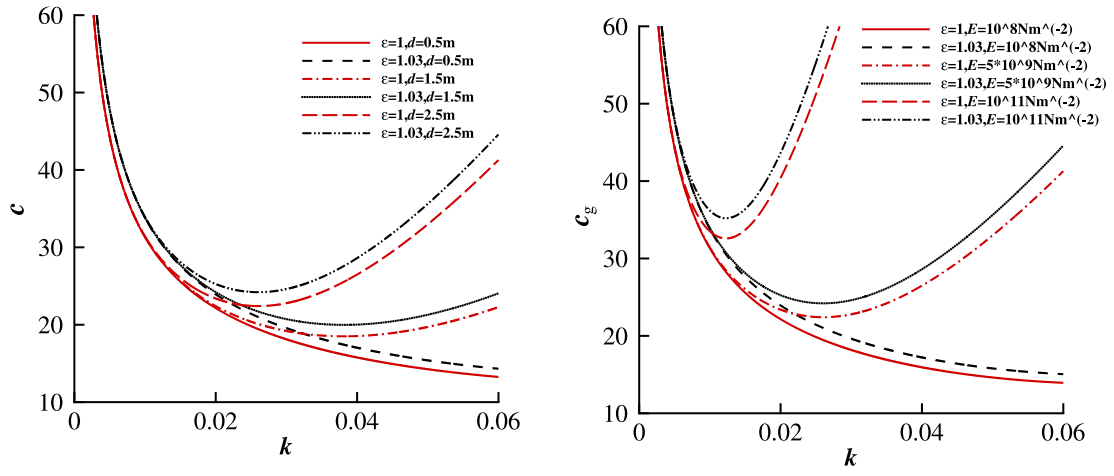

(a) Different values of d (b) Different values of E

Fig. 4. The phase speed $c(k)$ and group speed $c_g(k)$ in deep water versus the wave number k for different values.

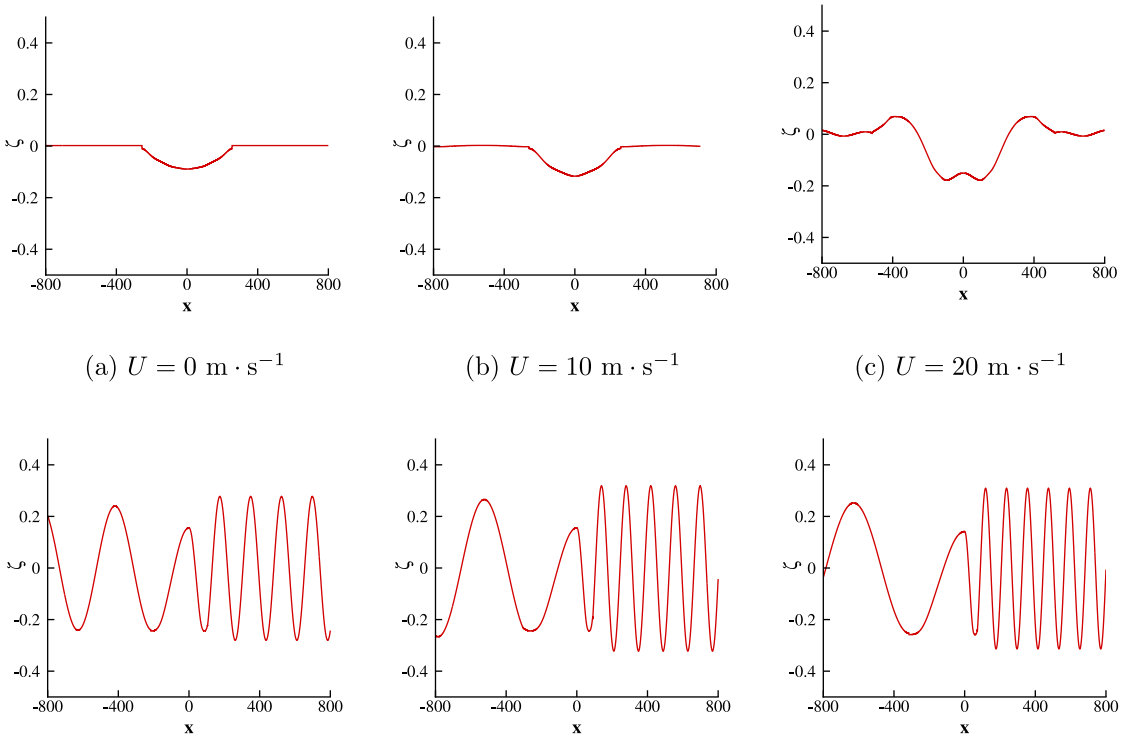

(a) $U = 0\ \mathrm{m}\cdot\mathrm{s}^{-1}$ (b) $U = 10\ \mathrm{m}\cdot\mathrm{s}^{-1}$ (c) $U = 20\ \mathrm{m}\cdot\mathrm{s}^{-1}$

(d) $U = 25\ \mathrm{m}\cdot\mathrm{s}^{-1}$ (e) $U = 30\ \mathrm{m}\cdot\mathrm{s}^{-1}$ (f) $U = 35\ \mathrm{m}\cdot\mathrm{s}^{-1}$

Fig. 5. Variation of the hydroelastic wave profiles versus x for different current speed U.

or an floating ice sheet under a localized load. As U approaches $c_{\min}$, symmetric decaying oscillations appear gradually in the upstream region ($x > 0$) and in the downstream region ($x < 0$). Moreover, we can find that the amplitude of the plate deflection increases gradually in the vicinity of the load with U.

As $U > c_{\min}$, the hydroelastic waves and the gravity waves occur far away from the load. As shown in Fig. 5, there are two wave systems: one with the shorter wavelength in the upstream region ($x > 0$) and the other with the longer

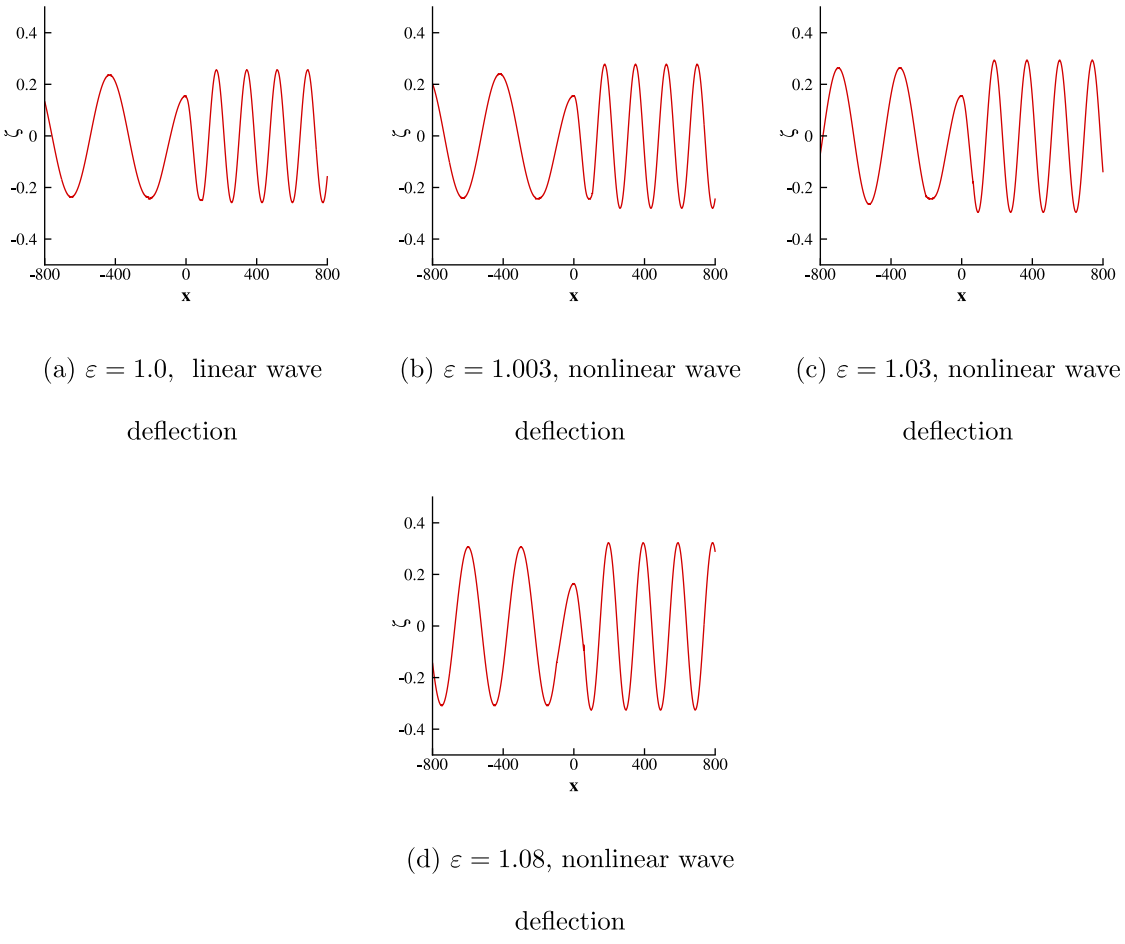

(a) $\varepsilon = 1.0$, linear wave deflection

(b) $\varepsilon = 1.003$, nonlinear wave deflection

(c) $\varepsilon = 1.03$, nonlinear wave deflection

(d) $\varepsilon = 1.08$, nonlinear wave deflection

Fig. 6. Variation of the hydroelastic wave profiles versus x for different value of the dimensionless frequency ε on the current speed $U = 25$ m s^{-1}.

Table 1
The total residual square error $\varepsilon_m^{\mathrm{T}}$ for different approximation order m with $c_0 = -0.1$.

m	ϵ_m^T
1	1.578
2	2.165×10^{-2}
3	2.730×10^{-4}
4	1.115×10^{-6}
6	3.216×10^{-8}

wavelength in the downstream region ($x < 0$). As U increases continuously, more waves in the leading region (i.e., the hydroelastic waves) appear and their wavelength decreases, while the waves in the trailing region (i.e., the gravity waves) become less and the wavelength of the gravity waves increases. It is shown that the hydroelastic and the gravity waves play leading roles in the upstream and downstream regions, respectively. Further, the amplitude of the waves in the leading and trailing regions firstly increase and then decrease with the current velocity U.

Fig. 6 shows the variation of the wave deflection with the increasing dimensionless parameter ε. Taking $U = 25$ m s^{-1} as an example, when ε increases from 1.0 to 1.08, the hydroelastic waves in the leading region ($x > 0$) become less and their wavelength increases, while more gravity waves in trailing region ($x < 0$) appear and the wavelength of the gravity waves decreases. Moreover, it is found that the wave amplitudes of the hydroelastic waves and the gravity waves increase gradually as the dimensionless parameter ε increases.

Further, we compare the nonlinear solution for the wave profiles with the linear one. It can be seen from Fig. 6 that the linear wave amplitudes ($\varepsilon = 1$) of the hydroelastic waves in the leading region and the gravity waves in trailing region

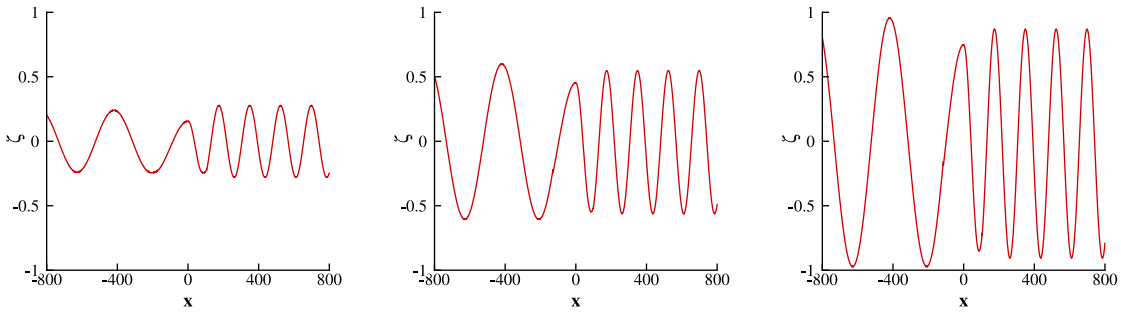

(a) $H = 0.2$ m (b) $H = 0.5$ m (c) $H = 0.8$ m

Fig. 7. Variation of the hydroelastic wave profiles versus x for different wave amplitudes H on the current speed $U = 25$ m s^{-1}.

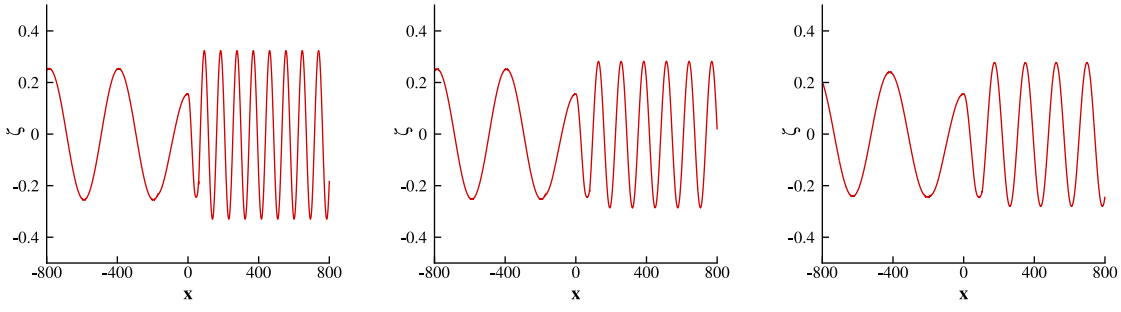

(a) $d = 1.5$ m (b) $d = 2.0$ m (c) $d = 2.5$ m

Fig. 8. Variation of the hydroelastic wave profiles versus x for different value of the plate thickness d on the current speed $U = 25$ m s^{-1}.

become smaller than the corresponding nonlinear ones ($\varepsilon > 1$). Thus, if the linear dispersion relation is used or the linear potential theory is used to study the nonlinear water waves, we will underestimate the variations of the wave deflection.

Figs. 7 and 8 show the wave deflections for different wave amplitudes H and different plate thicknesses d, respectively. Taking $U = 25$ m s^{-1} as an example, we consider the effects of wave amplitude on the elastic plate by increasing H from 0.2 m to 0.8 m as shown in Fig. 7. The amplitudes of the hydroelastic waves in the leading region and the gravity waves in the trailing region increase significantly with an increasing H. However, with the increase of plate thickness d from 1.5 m to 2.5 m, the amplitudes of the waves in the whole region decrease correspondingly as shown in Fig. 8. The reason is that the thickness of thin plate would have some effects on the elastic plate resistance. Further, with a large value of d in Fig. 8, the hydroelastic waves become less significantly and their wavelength increases, while the wavelength of the gravity waves has not changed significantly. However, the wavelengths of the hydroelastic and the gravity waves do not change with large value of H, as demonstrated in Fig. 7.

5. Conclusions

The steady-state and nonlinear hydroelastic waves generated by a moving load in a uniform current is studied analytically. The approximate nonlinear dispersion relation shows that there is a larger minimal phase speed than that of the linear one. In the frame of the HAM, we construct appropriate solution expressions for the unknown variables by comparing the relative current speed and the minimal phase speed, and the analytic solutions indicate that the steady wave system depends on the relationship between the two speeds. When the relative current speed is greater than the minimal phase speed, the hydroelastic waves and the gravity waves play leading roles in the upstream and downstream regions, respectively. If the relative current speed is far less than the minimal phase speed, there is no steady wave generated and the plate deflection is symmetric about the localized load.

As the nonlinearity increases, the wave amplitudes of both the gravity and the hydroelastic waves increase. The results obtained here demonstrate that the relative current speed and the approximate nonlinear dispersion relation have important effects on the steady-state hydroelastic response. In addition, the wave deflections increase greatly as the incident wave amplitude increases, while the plate thickness has an opposite effect on the wave deflections. Those

results obtained here can help us further understand that steady-state hydroelastic interaction between the VLFS or an floating ice sheet generated by moving vehicles or aircrafts in the real ocean.

Declaration of competing interest

There is no conflict of Interest.

Data availability

No data was used for the research described in the article.

Acknowledgments

This research was financially supported by the National Natural Science Foundation of China under Grant No. 11872239 and Qingdao Postdoctoral Applied Research Project, China under Grant No. 020022034. The authors would like to thank all the anonymous reviewers and the editor for their constructive comments which lead to the improvement of the original manuscript.

Appendix A. Detailed derivations for Eqs. (3) and (4)

In the earth-fixed coordinates, the nonlinear kinematic boundary and dynamic boundary conditions on the unknown plate–water interface ($z = \zeta(x, t)$) read

$$\frac{\partial \zeta}{\partial t} + \frac{\partial \phi}{\partial x}\frac{\partial \zeta}{\partial x} + U_0\frac{\partial \zeta}{\partial x} - \frac{\partial \phi}{\partial z} = 0, \tag{A.1}$$

$$\rho\left[\frac{\partial \phi}{\partial t} + \frac{1}{2}\left(|\nabla\phi|^2 + U_0^2\right) + U_0\frac{\partial \phi}{\partial x} + g\zeta\right] + P_e + P_{ext} = 0, \tag{A.2}$$

where P_e is the pressure at the plate—water interface and P_{ext} the external pressure distribution of a localized load at the coordinate origin. It is noted that the term $\frac{1}{2}U_0^2$ in Eq. (A.2), being independents of time and distance, can be removed by re-defining the velocity potential [26] and is omitted hereinafter.

The pressure in Eq. (A.2) is based on the Euler–Bernoulli beam theory as follows

$$P_e = D\nabla^4\zeta + M_e\frac{\partial^2 \zeta}{\partial t^2}. \tag{A.3}$$

The last term in the right-hand side of Eq. (A.3) is the plate acceleration term. We can neglect it when the wavelength of the surface displacement is much larger than the ice thickness [3,13]. Substituting Eq. (A.3) into Eq. (A.2) yields the full form of the dynamic boundary condition as

$$\frac{\partial \phi}{\partial t} + \frac{1}{2}|\nabla\phi|^2 + U_0\frac{\partial \phi}{\partial x} + g\zeta + \frac{1}{\rho}\left(D\nabla^4\zeta + P_{ext}\right) = 0, \tag{A.4}$$

In this paper, we are devoted to the study on the steady hydroelastic waves. We take the coordinate system oxz fixed on the moving load, then the boundary conditions (A.1) and (A.4) are transformed as

$$\frac{\partial \phi}{\partial x}\frac{\mathrm{d}\zeta}{\mathrm{d}x} + U\frac{\mathrm{d}\zeta}{\mathrm{d}x} - \frac{\partial \phi}{\partial z} = 0, \qquad (z = \zeta(x)), \tag{A.5}$$

$$f + U\frac{\partial \phi}{\partial x} + g\zeta + \frac{1}{\rho}\left(D\frac{\mathrm{d}^4\zeta}{\mathrm{d}x^4} + P_{ext}\right) = 0, \qquad (z = \zeta(x)), \tag{A.6}$$

where $U = U_0 - V_0$.

Noted that Eq. (A.5) contains only one linear term for the velocity potential $\phi(x, z)$. If we choose the solo linear term as the corresponding linear operator in the frame of HAM, this operator would affect the convergence of approximate solutions as illustrated by Liao [20] for some examples. Taking an operator $U\frac{\mathrm{d}}{\mathrm{d}x}$ on Eq. (A.6), then substituting Eq. (A.5) into the transformed Eq. (A.6), we have a combined boundary condition as follows

$$U^2\frac{\partial^2 \phi}{\partial x^2} + g\frac{\partial \phi}{\partial z} + U\frac{\partial f}{\partial x} - g\frac{\partial \phi}{\partial x}\frac{\mathrm{d}\zeta}{\mathrm{d}x} + \frac{U}{\rho}\left(D\frac{\mathrm{d}^5\zeta}{\mathrm{d}x^5} + \frac{\mathrm{d}P_{ext}}{\mathrm{d}x}\right) = 0, (z = \zeta(x)). \tag{A.7}$$

It is noted that there are two linear terms for $\phi(x, z)$.

Based on the nonlinear boundary condition Eqs. (A.7) and (A.6), the left-hand sides of Eqs. (A.7) and (A.6) are defined as two nonlinear operators $\mathcal{N}_1[\cdot,\cdot]$ and $\mathcal{N}_2[\cdot,\cdot]$, respectively, as shown in Eqs. (3) and (4).

Appendix B. Expressions of high-order deformation equations in the HAM

Let

$$\eta^n = \left(\sum_{i=1}^{+\infty} \zeta_i q^i\right)^n = \sum_{i=n}^{+\infty} \mu_{n,i} q^i. \tag{B.1}$$

According to the solution expression of every order velocity potential $\phi_m(x,z)$(20), we find that the independent variables x and z in every term of $\phi_m(x,z)$(20) are separable. So, for the unknown boundary $z = \eta(x;q)$, the function $\phi_m(x,z)$ can be expanded into the following Maclaurin series based on Eq. (B.1)

$$\begin{aligned}\phi_m(x,z) &= \phi_{1,m}(x)\phi_{2,m}(z) = \phi_{1,m}(x)\sum_{n=0}^{+\infty}\frac{1}{n!}\frac{\mathrm{d}^n\phi_{2,m}}{\mathrm{d}z^n}\Big|_{z=0} z^n \\ &= \phi_{1,m}(x)\sum_{n=0}^{+\infty}\left(\frac{1}{n!}\frac{\mathrm{d}^n\phi_{2,m}}{\mathrm{d}z^n}\Big|_{z=0}\right)\left(\sum_{i=n}^{+\infty}\mu_{n,i}q^i\right) \\ &= \sum_{i=0}^{+\infty}\psi_{m,i}q^i,\end{aligned} \tag{B.2}$$

where

$$\psi_{m,i} = \phi_{1,m}(x)\sum_{n=0}^{i}\left(\frac{1}{n!}\frac{\mathrm{d}^n\phi_{2,m}}{\mathrm{d}z^n}\Big|_{z=0}\right)\mu_{n,i}. \tag{B.3}$$

Thus we have, on $z = \eta(x;q)$,

$$\Phi(x,\eta;q) = \sum_{m=0}^{+\infty}\phi_m(x,\eta)q^m = \sum_{m=0}^{+\infty}\left(\sum_{i=0}^{+\infty}\psi_{m,i}q^i\right)q^m = \sum_{m=0}^{+\infty}\varphi_m q^m, \tag{B.4}$$

where

$$\varphi_m = \sum_{i=0}^{m}\psi_{m-i,i}. \tag{B.5}$$

Substituting the two series in Eqs. (B.4) and (13) into the zeroth-order deformation Eqs. (8) and (9), and then equating the like-power of the embedding parameter q, we can obtain, with the aid of HAM, the high-order deformation Eqs. (15) and (16) for which the detailed expressions are given by

$$\begin{aligned}\Delta^{\phi}_{m-1} &= U^2\frac{\mathrm{d}^2\varphi_{m-1}}{\mathrm{d}x^2} + g\bar{\varphi}_{m-1} - U\sum_{n=0}^{m-1}\left(\frac{\mathrm{d}\varphi_n}{\mathrm{d}x}\frac{\mathrm{d}^2\varphi_{m-1-n}}{\mathrm{d}x^2} + \bar{\varphi}_n\frac{\mathrm{d}\bar{\varphi}_{m-1-n}}{\mathrm{d}x}\right) \\ &\quad + \frac{U}{\rho}\left(D\frac{\mathrm{d}^5\zeta_{m-1}}{\mathrm{d}x^5} + \frac{\mathrm{d}P_{\mathrm{ext}}}{\mathrm{d}x}\right) - g\sum_{n=0}^{m-1}\frac{\mathrm{d}\varphi_n}{\mathrm{d}x}\frac{\mathrm{d}\zeta_{m-1-n}}{\mathrm{d}x}, \qquad (m\geq 2),\end{aligned} \tag{B.6}$$

$$\begin{aligned}\Delta^{\zeta}_{m-1} &= U\frac{\mathrm{d}\varphi_{m-1}}{\mathrm{d}x} + \frac{1}{2}\sum_{n=0}^{m-1}\left(\frac{\mathrm{d}\varphi_n}{\mathrm{d}x}\frac{\mathrm{d}\varphi_{m-1-n}}{\mathrm{d}x} + \bar{\varphi}_n\bar{\varphi}_{m-1-n}\right) + g\zeta_{m-1} \\ &\quad + \frac{1}{\rho}\left(D\frac{\mathrm{d}^4\zeta_{m-1}}{\mathrm{d}x^4} + P_{\mathrm{ext}}\right), \qquad (m\geq 2),\end{aligned} \tag{B.7}$$

$$\Delta^{\phi}_0 = U^2\frac{\mathrm{d}^2\varphi_0}{\mathrm{d}x^2} + g\bar{\varphi}_0 - U\left(\frac{\mathrm{d}\varphi_0}{\mathrm{d}x}\frac{\mathrm{d}^2\varphi_0}{\mathrm{d}x^2} + \bar{\varphi}_0\frac{\mathrm{d}\bar{\varphi}_0}{\mathrm{d}x}\right) + \frac{U}{\rho}\frac{\mathrm{d}P_{\mathrm{ext}}}{\mathrm{d}x}, \tag{B.8}$$

$$\Delta^{\zeta}_0 = U\frac{\mathrm{d}\varphi_0}{\mathrm{d}X} + \frac{1}{2}\left[\left(\frac{\mathrm{d}\varphi_0}{\mathrm{d}x}\right)^2 + \bar{\varphi}_0^2\right] + \frac{P_{\mathrm{ext}}}{\rho}, \tag{B.9}$$

$$S_{m-1} = \sum_{i=0}^{m-2} g\left(L_0\frac{\mathrm{d}^2\psi_{m-1-i,i}}{\mathrm{d}x^2} + \Gamma_{m-1-i,i}\right), \tag{B.10}$$

$$\bar{S}_m = \sum_{i=1}^{m-1} g\left(L_0\frac{\mathrm{d}^2\psi_{m-i,i}}{\mathrm{d}x^2} + \Gamma_{m-i,i}\right), \tag{B.11}$$

where

$$\bar{\varphi}_{m-1} = \sum_{i=0}^{m-1} \gamma_{m-1-i,i}, \tag{B.12}$$

$$\Gamma_{m-i,i} = \sum_{n=0}^{i} \frac{1}{n!} \left(\frac{\partial^{n+1} \phi_{m-i}}{\partial z^{n+1}} \Big|_{z=0} \right) \mu_{n,i}. \tag{B.13}$$

Appendix C. Analytical expressions for the coefficients in the solutions

$$\alpha_{i,0,1} = \frac{\upsilon}{C_0 \bar{L}_0} \left[1 + \overline{\gamma} - \frac{4C_0 \overline{P}_0 (259 + 175238\overline{\gamma} + 11406979\overline{\gamma}^2)}{225 e \pi^2 (1 + 81\overline{\gamma})(1 + 625\overline{\gamma})} \right], \tag{C.1}$$

$$\alpha_{i,1,1} = -\frac{4C_0 \overline{P}_0 \upsilon}{(1 - \bar{L}_0) e \pi^2} + \frac{\upsilon}{\bar{L}_0} \left[1 + \overline{\gamma} - \frac{4C_0 \overline{P}_0 (259 + 175238\overline{\gamma} + 11406979\overline{\gamma}^2)}{225 e \pi^2 (1 + 81\overline{\gamma})(1 + 625\overline{\gamma})} \right], \tag{C.2}$$

$$\left\{ \alpha_{i,1,2}, \alpha_{i,1,3}, \alpha_{i,1,4}, \alpha_{i,1,5} \right\} = \frac{C_0 \overline{P}_0 \upsilon}{e \pi^2} \left\{ \frac{1}{1 - 2\bar{L}_0}, -\frac{4}{9(1 - 3\bar{L}_0)}, \frac{1}{4(1 - 4\bar{L}_0)}, -\frac{4}{25(1 - 5\bar{L}_0)} \right\}, \tag{C.3}$$

$$\beta_{i,1,0} = H \left[\frac{2C_0 \overline{P}_0}{3e} + \frac{\overline{H}}{2C_0 \bar{L}_0} \left(1 + \overline{\gamma} - \frac{4C_0 \overline{P}_0 (259 + 175238\overline{\gamma} + 11406979\overline{\gamma}^2)}{225 e \pi^2 (1 + 81\overline{\gamma})(1 + 625\overline{\gamma})} \right)^2 \right], \tag{C.4}$$

$$\beta_{i,1,1} = H \left[\frac{4C_0 \overline{P}_0}{1 + \overline{\gamma}} \left(\frac{1}{e \pi^2} - \frac{259 + 175238\overline{\gamma} + 11406979\overline{\gamma}^2}{225 e \pi^2 (1 + 81\overline{\gamma})(1 + 625\overline{\gamma})} \right) + 1 \right], \tag{C.5}$$

$$\left\{ \beta_{i,1,2}, \beta_{i,1,3}, \beta_{i,1,4}, \beta_{i,1,5} \right\} = \frac{C_0 \overline{P}_0 H}{e \pi^2} \left\{ -\frac{1}{1 + 16\overline{\gamma}}, \frac{4}{9(1 + 81\overline{\gamma})}, -\frac{1}{4(1 + 256\overline{\gamma})}, \frac{4}{25(1 + 625\overline{\gamma})} \right\} \tag{C.6}$$

where

$$\upsilon = HU, \qquad \overline{\gamma} = \gamma k^4, \qquad \overline{P}_0 = \frac{P_0}{\rho g H}, \qquad \bar{L}_0 = k L_0, \qquad \overline{H} = kH. \tag{C.7}$$

References

[1] J.T. Wilson, Moving loads on floating ice sheets, Technical Report, University of Michigan Research Rep. UMRL Project 2432, 1958.
[2] J.W. Davys, R.J. Hosking, A.D. Sneyd, Waves due to a steadily moving source on a floating ice plate, J. Fluid Mech. 158 (1985) 269–287.
[3] R.M.S.M. Schulkes, A.D. Sneyd, Time-dependent response of floating ice to a steadily moving load, J. Fluid Mech. 186 (1988) 25–46.
[4] F. Milinazzo, M. Shinbrot, N.W. Evans, A mathematical analysis of the steady response of floating ice to the uniform motion of a rectangular load, J. Fluid Mech. 287 (1995) 173–197.
[5] V.A. Squire, R.J. Hosking, A.D. Kerr, P.J. Langhorne, Moving loads on ice plates, Kluwer Academic Publishers, Dordrecht, 1996.
[6] D.Q. Lu, H. Zhang, Flexural-gravity wave resistances due to a surface-moving line source on a fluid covered by a thin elastic plate, Theor. Appl. Mech. Lett. 3 (2) (2013) 022002.
[7] D.Q. Lu, C.Z. Sun, Transient flexural-and capillary-gravity waves due to disturbances in two-layer density-stratified fluid, J. Hydrodyn. 25 (3) (2013) 23–31.
[8] J.S. Li, D.Q. Lu, Flexural-gravity wave resistances due to a moving point source on 2-d infinite floating beam, J. Hydrodyn. 29 (6) (2017) 1000–1009.
[9] M.H. Meylan, The time-dependent vibration of forced floating elastic plates by eigenfunction matching in two and three dimensions, Wave Motion 88 (2019) 21–33.
[10] Y.Z. Xue, L.D. Zeng, B.Y. Ni, A.A. Korobkin, T.I. Khabakhpasheva, Hydroelastic response of an ice sheet with a lead to a moving load, Phys. Fluids 33 (3) (2021) 037109.
[11] E. Părău, F. Dias, Nonlinear effects in the response of a floating ice plate to a moving load, J. Fluid Mech. 460 (2002) 281–305.
[12] F. Bonnefoy, M.H. Meylan, P. Ferrant, Nonlinear higher order spectral solution for a two-dimensional moving load on ice, J. Fluid Mech. 621 (2009) 215–242.
[13] E.I. Părău, J.M. Vanden-Broeck, Three-dimensional waves beneath an ice sheet due to a steadily moving pressure, Phil. Trans. R. Soc. A 369 (2011) 2973–2988.
[14] P. Guyenne, E.I. Părău, Forced and unforced flexural-gravity solitary waves, Procedia IUTAM 11 (2014) 44–57.
[15] P.I. Plotnikov, J.F. Toland, Modelling nonlinear hydroelastic waves, Phil. Trans. R. Soc. A 369 (2011) 2942–2956.
[16] S.K. Mohanty, J. Bhattacharjee, T. Sahoo, Time dependent flexural gravity waves in the presence of current, J. Fluids Struct. 45 (2) (2014) 28–49.
[17] D.Q. Lu, R.W. Yeung, Hydroelastic waves generated by point loads in a current, Int. J. Offshore Polar Eng. 25 (1) (2015) 8–12.
[18] S.J. Liao, The proposed homotopy analysis technique for the solution of nonlinear problems (Ph.D. thesis), Shanghai Jiao Tong University, 1992.
[19] S.J. Liao, Beyond Perturbation: Introduction To the Homotopy Analysis Method, CRC Press, Boca Raton, 2004.
[20] S.J. Liao, Homotopy Analysis Method in Nonlinear Differential Equations, Higher Education Press, Beijing, 2012.
[21] Y. Wu, K.F. Cheung, Homotopy solution for nonlinear differential equations in wave propagation problems, Wave Motion 46 (2009) 1–14.

[22] D.L. Xu, Z.L. Lin, S.J. Liao, M. Stiassnie, On the steady-state fully resonant progressive waves in water of finite depth, J. Fluid Mech. 710 (2012) 379–418.
[23] Z. Liu, S.J. Liao, Steady-state resonance of multiple wave interactions in deep water, J. Fluid Mech. 742 (2014) 664–700.
[24] Z. Liu, D. Xie, Finite-amplitude steady-state wave groups with multiple near-resonances in finite water depth, J. Fluid Mech. 867 (2019) 348–373.
[25] J. Bhattacharjee, T. Sahoo, Interaction of current and flexural gravity waves, Ocean Eng. 34 (2007) 1505–1515.
[26] D.Q. Lu, On the initial values of kinematic and dynamic free-surface boundary conditions for water wave problems, J. Hydrodyn. 32 (5) (2020) 1024–1027, http://dx.doi.org/10.1007/s42241-020-0054-9.